Dibenzothiophene adsorption at boron doped carbon nanoribbons studied within density functional theory

P. López-Albarrán, P. Navarro-Santos, M. A. Garcia-Ramirez, and J. L. Ricardo-Chávez

Citation: Journal of Applied Physics **117**, 234301 (2015);
View online: https://doi.org/10.1063/1.4922452
View Table of Contents: http://aip.scitation.org/toc/jap/117/23
Published by the American Institute of Physics

Dibenzothiophene adsorption at boron doped carbon nanoribbons studied within density functional theory

P. López-Albarrán,[1] P. Navarro-Santos,[2,a)] M. A. Garcia-Ramirez,[3] and J. L. Ricardo-Chávez[4]

[1]*Facultad de Ingeniería en Tecnología de la Madera, Universidad Michoacana de San Nicolás de Hidalgo, Santiago Tapia 403, CP 58000, Morelia, Michoacán, Mexico*
[2]*Instituto de Investigaciones Químico-Biológicas, Universidad Michoacana de San Nicolás de Hidalgo, Santiago Tapia 403, CP 58000, Morelia, Michoacán, Mexico*
[3]*Research Centre for Innovation in Aeronautical Engineering, Universidad Autónoma de Nuevo León, Ciudad Universitaria, San Nicolás de los Garza, CP 66451 Nuevo León, Mexico*
[4]*Instituto Potosino de Investigación Científica y Tecnológica, Camino a la Presa San José 2055, Lomas 4[a]sección, CP 78216, San Luis Potosí, S. L. P., Mexico*

(Received 8 January 2015; accepted 16 May 2015; published online 15 June 2015)

The adsorption of dibenzothiophene (DBT) on bare and boron-doped armchair carbon nanoribbons (ACNRs) is being investigated in the framework of the density functional theory by implementing periodic boundary conditions that include corrections from dispersion interactions. The reactivity of the ACNRs is characterized by using the Fukui functions as well as the electrostatic potential as local descriptors. Non-covalent adsorption mechanism is found when using the local Perdew-Becke-Ernzerhof functional, regardless of the DBT orientation and adsorption location. The dispersion interactions addition is a milestone to describe the adsorption process. The charge defects introduced in small number (i.e., by doping with B atoms), within the ACNRs increases the selectivity towards sulfur mainly due to the charge depletion at B sites. The DBT magnitude in the adsorption energy shows non-covalent interactions. As a consequence, the configurations where the DBT is adsorbed on a BC_3 island increase the adsorption energy compared to random B arrangements. The stability of these configurations can be explained satisfactorily in terms of dipole interactions. Nevertheless, from the charge-density difference analysis and the weak Bader charge-distribution interactions cannot be ruled out completely. This is why the electronic properties of the ribbons are analyzed in order to elucidate the key role played by the B and DBT states in the adsorbed configurations. © *2015 AIP Publishing LLC*. [http://dx.doi.org/10.1063/1.4922452]

I. INTRODUCTION

Organosulfur compounds such as thiophenes are pollutants present in undesirable proportions in many petrochemical industry derivatives such as gasoline, highway diesel, and jet fuel.[1,2] These compounds, being the heavier ones the dibenzothiophene (DBT) and its alkyl derivatives show a major drawback to refineries as those present a rather low reactivity in the hydrodesulfurization processes (HDS) due to both of them require high temperature and pressure to increase the removal efficiency.[3–6] A direct environmental impact occurs when lower sulfur levels are reached due to the increasing operation costs for HDS, alternative desulfurization methods are foreseen. A promising approach relies to use molecular sieves to adsorb the sulfur compounds.[7] In this direction, several materials such as hydrogels,[8] alumina,[9] zeolites,[10] and activated carbon[11–13] have been tested as adsorbents with poor results.

An alternative approach that we are pursuing in this work is the use of nanostructured materials with high adsorption capacity. An attractive candidate as adsorbent material is nanostructured carbon. This material has quite a few key characteristics, one of them relies into adopt a set of geometrical structures leading to a large variety of materials with novel physical and chemical properties. Few of these carbon-based aromas prone to study are graphene, carbon nanotubes (CNTs), carbon nanoribbons (CNRs), among others. Those have attracted a lot of interest due to the feasibility of tailoring the structural and electronic properties as required for technological applications.[14–17] However, previous work shows that adsorption of thiophene and DBT on bare graphene and CNTs was not promising due to the limited reactivity of both surfaces.[18] The main aim in this work is to demonstrate, based on theoretical analyses, that it is possible to tune the reactivity of these materials, specifically, CNRs through a selective doping in low concentrations and by controlling the relative arrangement of the dopant atoms. In order to reach such goal, we are focusing into propose novel structures with suitable adsorption properties that encompass a broad variety of characteristics for sensing applications.

CNRs are long and narrow an atom thick-sheets made out of graphene. Those are passivated at the edges with hydrogen atoms. In function of the cutting edge direction, two topological conformations are obtained: armchair and zigzag according to the edges nature. By following a usual convention,[19–23] the armchair CNRs (ACNRs) are classified by the number of dimer lines through the ribbon width. When dimer lines are

[a)]Author to whom correspondence should be addressed. Electronic mail: pnavarrosa@conacyt.mx

zigzag chains, these nanoribbons are referred as zigzag CNRs. Due to their finite dimension, CNRs have a peculiar set of electronic states close to the edges that play a key role within the reactivity and electronic properties.[19–21,23–25] In this matter, CNRs seem more appropriate than graphene and CNTs to develop an adsorbent material by tuning its reactivity through functionalization and doping. According to a broad bibliography survey, this study is the first report of the organosulfur compounds adsorption on ACNRs to tune the reactivity properties of boron-doped ACNRs (B-ACNRs). Our research work has the following distribution: Section II describes the methodology implemented to perform the simulations. In Sec. III, a discussion on the structural and energetic stability of the adsorption complexes as well as the main results are shown. Finally, the conclusions of this study are discussed in Sec. IV.

II. COMPUTATIONAL METHODS

By following the usual convention,[26] the size of the ACNRs is denoted as $M \times N$, where M is the number of rows along the transverse (x) direction, and N represents the number of rows along the periodic (z) direction as shown in Fig. 1. In this work, we restricted our study to a size of 16×4 ACNRs, although the results obtained from this study can be applied to larger systems. The B-ACNRs are obtained through the substitution of six carbon atoms by boron atoms in the bare 16×4 ACNRs (less than 10% doping). Three geometrical arrangements of the boron atoms are analyzed and depicted in Figs. 1(c) to 1(e). In here, (c) depicts a BC_3 island placed at the center of the ribbon, where it is denoted as ACNR-*C*; at (d), a BC_3 island is placed at an edge of the ribbon denoted as ACNR-*E*; and finally, at (e) a random distribution of boron atoms over the entire ribbon is denoted as ACNR-*R*.

The ACNRS and B-ACNRs structures are relaxed self consistently at DFT level without imposing any symmetry constraint by using the conjugate gradient method, until the force on each atom was lower than 0.01 eV/Å. The numerical analyses are performed by using the "Vienna *Ab initio* Simulation Package" (VASP).[27–29] In here, the DFT Kohn-Sham equations by using a plane-wave basis are set. We selected the projector-augmented wave (PAW) method to use the interactions between ionic cores and valence electrons.[30,31] It is also included the electronic exchange and correlation effects by using the Perdew-Burke-Ernzerhof (PBE) gradient-corrected functional with a long-range dispersion correction through the Grimme's D2 method.[32,33] As VASP uses a periodic approach to electronic structures, the ribbons are placed in an orthorhombic cell being periodic in the z direction of the ribbon. By having a minimum space of 10 Å along the non-periodic directions, it is possible to reduce spurious interactions between neighbor system images. These dimensions are optimized to keep the cell total stress close to a minimum. According to cell dimensions, a few k-points are needed to sample the Brillouin zone in reciprocal space. As a result, a grid of $1 \times 15 \times 1$ points the Monkhorst-Pack and a plane-wave cutoff energy of 500 eV represents a good compromise between precision and computing time for the optimization of the electronic density at each relaxation step. As the ACNRs do not show significant magnetization effects,[23,26] whole analyses performed do not include spin polarization solutions.

In order to study the reactivity of the bare and B-ACNRs towards DBT adsorption, we have located the

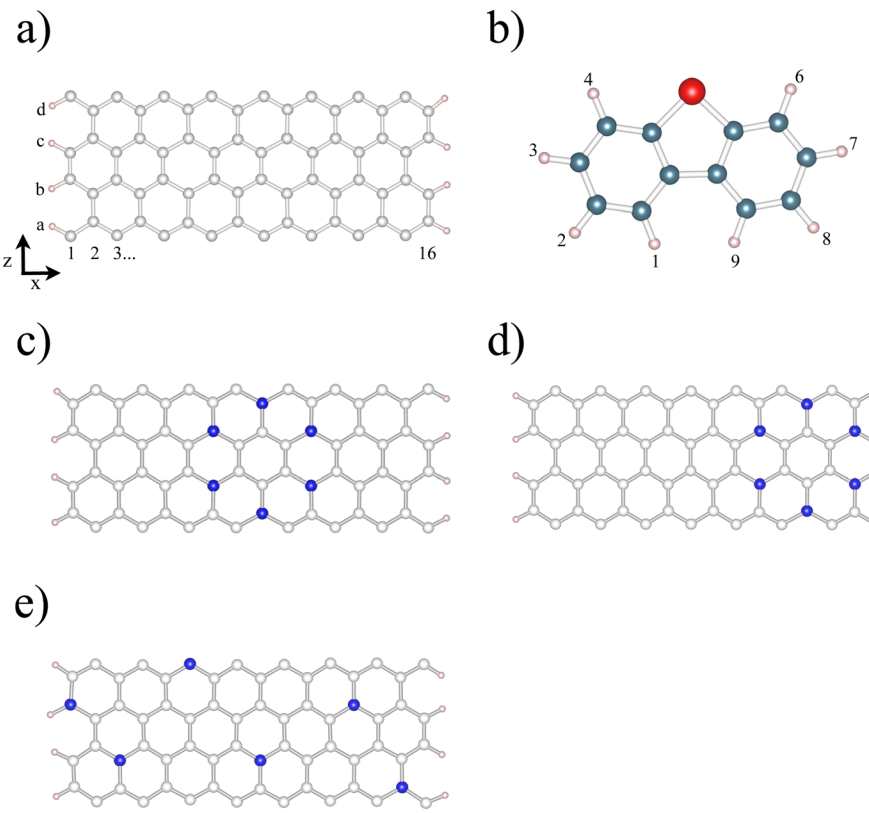

FIG. 1. Optimized geometry of: (a) bare ACNR, (b) dibenzothiophene, (c) ACNR-*C*, (d) ACNR-*E*, and (e) ACNR-*R*. Blue and grey balls represent boron and carbon atoms, respectively, in the ACNRs nanostructures, while red and blue balls represent sulfur and carbon atoms in the dibenzothiophene molecule.

most active adsorption sites on the ribbon surface by using an appropriate reactivity descriptor. However, there is not-a-criteria to accomplish this task without prior knowing the adsorption mechanism. This is why, we selected two reactivity descriptors that are able to cover both covalent and non-covalent interactions. The first one is the electrostatic or Hartree potential

$$V(\mathbf{r}) = \sum_A \frac{Z_A}{|\mathbf{R}_A - \mathbf{r}|} - \int \frac{\rho(\mathbf{r}')\, d\mathbf{r}'}{|\mathbf{r}' - \mathbf{r}|} \tag{1}$$

that provided us with information on the nuclear and electronic charge distribution in the system.

The second one is the Fukui or frontier function, which is defined as the change of the electronic density with respect to number of electrons (N), considering the nuclei position fixed, i.e., constant external potential $v(r)$

$$f(r) = \left(\frac{\partial \rho(\mathbf{r})}{\partial N}\right)_{v(r)}. \tag{2}$$

Due to the discontinuity of the derivative expression with respect to N, the following three functions can be defined in a finite difference approximation:

$$f^+_{v,N}(r) = \rho_{v,N+1}(r) - \rho_{v,N}(r), \tag{3}$$

$$f^-_{v,N}(r) = \rho_{v,N}(r) - \rho_{v,N-1}(r), \tag{4}$$

$$f^0_{v,N}(r) = 0.5(\rho_{v,N+1}(r) - \rho_{v,N-1}(r)), \tag{5}$$

where $\rho_{v,N+1}(r)$, $\rho_{v,N}(r)$, and $\rho_{v,N-1}(r)$ are the electronic densities of the system with $N+1$, N, and N–1 electrons, respectively, all with the ground state geometry of the N electron system. Although the finite difference approximation to the Fukui functions works for a specific set of configurations, whilst for others is worthless to implement (i.e., full configuration interaction),[34] in most cases they are considered a reliable descriptor to indicate how the electron (incoming or outcoming) is redistributed in regions of the molecule.[35] Expressions (3)–(5) are, respectively, evaluated for: nucleophilic attack, where a molecule gains an electron; electrophilic attack, where a molecule loses an electron; and for free radical attacks.[36] This treatment of chemical reactivity is based on the assumption that when molecules A and B interact in order to form a product AB a molecular densities-perturbation occurs.[37] As the electronic density contains all sort of information, the chemical reactivity has to be reflected within its sensitivity to perturbations. Moreover, the Fukui function is also defined as the initial response in $\rho_{v,N}(r)$ due to an infinitesimal perturbation in the total N, at constant external potential $v(r)$, and by measuring the $\rho_{v,N}(r)$ of the frontier orbitals (HOMO or LUMO) to a small change in the number of electrons N at fixed nuclei positions.[34,38,39] In this work, only the nucleophilic form of Fukui function, $f^+(r)$, is analyzed for the ACNRs to evaluate their reactivity and sensibility as function to an incoming charge. The $f^+(r)$ is obtained by applying the frozen core approximation within frontier orbital[40]

$$f^+(r) = |\phi^{LUMO}_{v,N}(r)|^2 = \rho^{LUMO}_{v,N}(r). \tag{6}$$

The electrostatic potential and the Fukui functions provide information on the local selectivity for donor-acceptor interactions. In here, the electrostatic potential describes the long-range non-covalent interactions.[41] The evaluation of the incoming charge distribution on nanoribbons states that "the Fukui function is strong while regions of a molecule are chemically softer than the regions where the Fukui function is weak. By invoking the hard and soft acid and bases (HSAB) principle[42] in a local sense, it is possible to establish the behavior of the different sites as a function of hard or soft reagents (adsorbates)."[34,38,43–45] In the adsorption processes, it is common to transfer a fraction of the electron charge. In here, the Fukui function is a boundary case that provided us with inside information of such processes.

The electrostatic potential is computed in VASP, while the Fukui functions are calculated by using the frozen-orbital approximation as referred above for the LUMO densities obtained also with VASP and visualized through the VESTA package.[46]

Several trial configurations are considered to study the DBT adsorption complexes on ACNRs and B-ACNRs for several DBT molecule orientations at active sites in the ribbons. These configurations are optimized for the bare ACNRs and B-ACNRs. The adsorption energies (E_A) are analyzed by using the following equation:

$$E_A = E_{complex} - (E_{ACNR} + E_{DBT}), \tag{7}$$

where $E_{complex}$ is the energy of the optimized DBT-(B-) ACNRs complex, E_{ACNR} is the energy of the optimized bare or B-doped ACNR, and E_{DBT} is the energy of the optimized DBT molecule in gas-phase.

III. RESULTS AND DISCUSSION

The ACNRs and B-ACNRs electronic properties have been previously studied in our group[26] by using a similar methodology as in the present research. It was found that B-ACNRs with BC_3 island conformations are more stable than random B arrangements. BC_3 conformations are always semiconducting independently of width and length due to a strong localization of the B states near the Fermi level. In here, random B arrangements are metallic due to the delocalization of the B states. Figure 1(a) depicts the optimized geometry of the bare 16×4 ACNR, while parts (c)–(e) show the optimized geometries of 16×4 ACNR-*C*, ACNR-*E*, and ACNR-*R*, respectively. The C–C bond lengths of B-ACNRs are between 1.41 and 1.44 Å, while B–C distances are 1.50 Å. In the BC_3 island conformation, the B–B separation is close to 2.89 Å, while in the random arrangement it can be as large as 6.27 Å. Figure 1(b) also shows the optimized geometry for the DBT molecule, which has a S–C bond length of 1.75 Å and C-C bond lengths of the order of 1.40 Å.

Table I lists the lattice supercell parameters by including corrections from dispersion interactions. From these results, we find that the calculations with dispersion corrections give us a few differences on lattice parameter up to 0.03 Å for the

TABLE I. Lattice parameters in Å and cohesive per atom (Gibbs free) energies in eV of the non-doped and B-doped ACNRs.

	Lattice parameters			Binding energy (δG)		
	PBE	DFT-D2	DFT-D3	PBE	DFT-D2	DFT-D3
Pristine	8.62	8.64	8.64	7.224 (0.003)	7.357 (−1.727)	7.318 (−1.738)
ACNR-C	8.69	8.72	8.72	7.003 (−0.291)	7.167 (−1.923)	7.118 (−1.918)
ACNR-E	8.73	8.72	8.71	7.008 (−0.297)	7.171 (−1.928)	7.122 (−1.923)
ACNR-R	8.71	8.72	8.71	6.983 (−0.272)	7.147 (−1.904)	7.102 (−1.902)

nanoribbon ACNR-*C* according to the analyses in which the PBE functional was used. In order to analyze the stability of those nanostructures, the energetic properties were also considered. Table I displays the cohesive energy per atom and the Gibbs free energy of the pristine and doped ACNRs. The cohesive energy (E_C) is the energy required to disassemble a system into each one of its parts. A bound (stable) system has a positive value of E_C, which represents the energy gained during the formation of the bound state. Similar trends are found within all our analyses performed. The E_C of the non-doped ACNR is higher than the B-doped ACNR independently of the boron distributions. The difference at the E_C (up to 2.4 eV/atom) between the non-doped and the B-doped ACNRs is obtained by using the PBE functional.

Table I displays that both the non-doped and B-doped ACNRs are stable as a graphene sheet. The B doping slightly reduces the cohesive energy compared to the pristine ACNRs. As shown elsewhere,[26] this reduction becomes less important when the system size increases. In particular, the energy reduces while the island is nearby the ribbon edge indicating that the formation of the BC_3 island[47] and the substitution on the edges[48,49] are keys to ACNRs stability routes. Table I also lists the Gibbs free formation energy (δG) of the ACNRs that is considered the relative stability of multicomponent systems such as those for ACNRs. The δG is given by

$$\delta G = E(x) + x_H\mu_H + x_B\mu_B + x_C\mu_C, \quad (8)$$

where $E(x)$ is the cohesive energy per atom of the ACNR, μ_H is the binding energy per atom of the singlet ground state of the H_2 molecule, μ_B is the binding energy per atom of the triplet ground state of the B_2 molecule, and μ_C is the cohesive energy per atom of the graphene sheet. x_i corresponds to the molar fraction of the different components (H, B, C), which satisfies $x_i = 1$. A negative value for δG represents a stable structure according to the constituent, whereas a positive value represents a metastable structure. From Table I, we can observe that results for the δG show similar trend for all the functionals used: ACNR-E > ACNR-C > ACNR-R. By finding the large difference in function of the non-doped ACNR employing the PBE functional (0.294 eV/atom), this stability is in agreement with the numerically analyzed binding energies. In addition, it is interesting to observe that the position of the BC_3 nanoisland has a subtle effect in the stability of those B-doped ACNRs (~50 meV/ atom).

In order to understand how the introduction of charge defects via boron doping modifies the chemical reactivity of the ribbons, it is divided into three sections as shown in Fig. 2. The computed electrostatic potential of the bare 16×4 ACNR, the B-doped 16×4 ACNR-*C*, and ACNR-*R* configurations is mapped on an isosurface of the charge density as

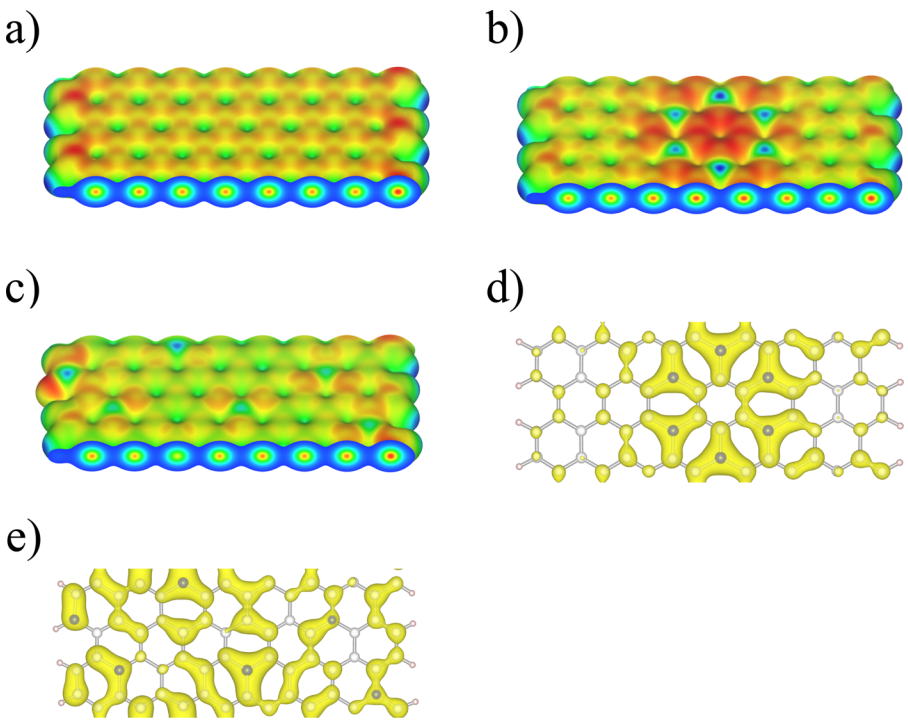

FIG. 2. The molecular electrostatic potential mapped at the electronic density isosurface (iso = 0.02 e^-/Bohr^3) for the (a) bare ACNR, (b) ACNR-*C*, (c) ACNR-*R*, respectively, and the isosurface (isovalue of 1×10^{-10} e^-/Bohr^3) of the Fukui function $f^+(r)$ of the ACNRs: (d) ACNR-*C* and (e) ACNR-*R*, respectively. Boron atoms are highlighted in (d) and (e) with blue spheres to facilitate their position in the nanoribbons.

TABLE II. Adsorption energy (in eV), bond distances (in Å), difference of energy between configurations 1 and 2 (in meV), and final orientation (perpendicular or tilted) of the most stable adsorption configuration of the DBT on pristine and B-doped ACNRs.

	1	2	Difference of energy between configurations 1 and 2	
Initial conformation	S⊥ACNR	H⊥ACNR		
Pristine ACNR	−0.23 $d_{C(b9)\text{-}S}$ (3.18 Å) $d_{C(b6)\text{-}H4}$ (3.04 Å) Perpendicular	−0.40 $d_{C(c9)\text{-}H1}$ (2.76 Å) $d_{C(c9)\text{-}H9}$ (2.80 Å) Perpendicular	170	
ACNR-*C*	−0.42 $d_{B(a9)\text{-}S}$ (2.92 Å) $d_{C(a7)\text{-}H4}$ (2.84 Å) Tilted (58.22°)	−0.38 $d_{B(b15)\text{-}H1}$ (2.70 Å) $d_{B(b15)\text{-}H9}$ (2.86 Å) Perpendicular	−40	(Near the most reactive site of the ACNR)
ACNR-*E*	−0.35 $d_{B(b16)\text{-}S}$ (3.11 Å) $d_{C(b13)\text{-}H4}$ (2.70 Å) Tilted (63.81°)	−0.33 $d_{B(b15)\text{-}H1}$ (2.84 Å) $d_{B(b11)\text{-}H9}$ (2.72 Å) Perpendicular	−20	(Near the most reactive site of the ACNR)
ACNR-*R*	−0.40 $d_{B(a11)\text{-}S}$ (3.09 Å) $d_{C(a9)\text{-}H4}$ (2.99 Å) Tilted (67.64°)	−0.34 $d_{B(d6)\text{-}H1}$ (2.70 Å) $d_{B(d6)\text{-}H9}$ (2.73 Å) Perpendicular	−60	(Near the most reactive site of the ACNR)

shown in Fig. 2. By following the usual convention, the coloring of the isosurfaces goes from red (negative) to green (neutral) and blue (positive) values.

Figure 2(a) shows the surface of the bare ACNR and the characteristic distribution of negative charge at the center of the C-C covalent bonds within a well-known localization effect of negative charge near the ribbon edges that intensifies the effect due to a charge transfer from the H atoms. Then, most of the bare ACNR surface would improve its reaction to electrophiles (for example, Lewis acids) at the C-C bridges. The substitution of some C with B atoms causes a redistribution of the ribbon charge as the B atom introduces charge depletion at its site or in some cases, charge accumulation on the carbon atoms near the boron atoms. Therefore, the charge redistribution depends on the relative B-B arrangement. In the case of a BC_3 island conformation, it is one of the most stable B-ACNRs and it is shown in part in Fig. 2(b). In here, there is a strong negative charge accumulation around the B atoms, with the most intense region localized at the central part of the ring. The B atoms would then accept nucleophiles (for example, Lewis bases), while the C-C bridges still accept electrophiles as in the case of the bare ACNR. Any incoming charge would then be distributed around the B atoms, as it is shown by the corresponding $f^+(r)$ in Fig. 2(d). More complicated charge redistribution occurs in the random B arrangement [shown in Fig. 2(c)], which tends to localize charge in the region surrounding the B atoms and strongly modifies the reactivity of the surface. In this case, any incoming charge would still be distributed and localized around the B atoms, as shown by the corresponding $f^+(r)$ in Fig. 2(e). These results give us insights of the regions where the B-doped ACNRs may redistribute the incoming charge.

Through the DBT electrostatic potential analysis,[50,51] we know that the most reactive sites are: the S atom, which can donate charge through its lone electron pairs and it is therefore a nucleophile, the aromatic rings, which can also donate charge and the hydrogen atoms that could accept charge. The S and aromatic C atoms are able to strongly interact with the B sites on the ribbon surface, while the H atoms rely on the C-C bridges. Despite these facts, we have decided to study several conformations in order to explore the affinity that the ribbon surface has to a set of different DBT orientations. The competitive DBT adsorption through the aromatic rings and hydrogen atoms might decrease the HDS efficiency processes because it is effective while complexes are formed through the sulfur atom.[52,53] A previous study[54] on the DBT adsorption on MoS_2 has shown that the preferred orientation is perpendicular to the surface only if it is adsorbed through the sulfur atom and parallel to the surface when it is adsorbed through the aromatic rings.

In order to cover the main adsorption pathways of DBT on the ribbon surface, we have considered the following cases. The first set is when adsorption takes place through the sulfur atom perpendicularly oriented to the surface (denoted as ⊥) and placed near the center (S⊥C) and edge (S⊥E) of the ribbon. A second set corresponds to the competitive case when DBT is adsorbed through the hydrogen atoms of the aromatic rings (denoted as H) near the center (H⊥C) and edge (H⊥E) of the ribbon. The third and last set of configurations is when DBT is parallel to the ribbon surface (denoted as ||). None of these configurations was found to be stable by using the local PBE functional. In contrast, all of them are stable at the semiempirical DFT-D2 level by varying the stability properties depending on the DBT

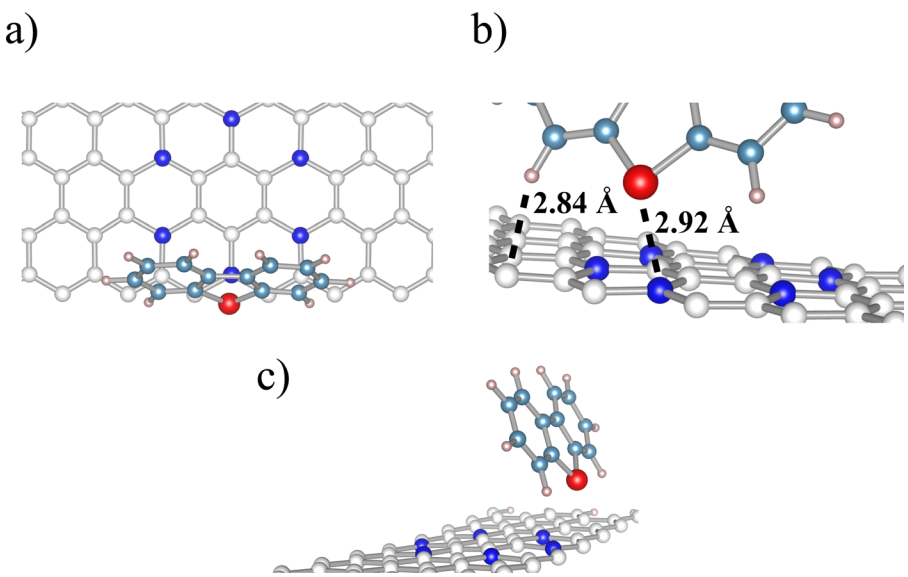

FIG. 3. Complexes formed for the DBT on the ACNR-*C* conformation. Light blue and gray balls represent carbon atoms, while boron and sulfur atoms are represented in dark blue and red colors, respectively.

orientation. This is why, all analyses as well as results are performed by using the DFT-D2 functional.

Table II shows the adsorption energy results, bond distances, and relative DBT–ribbon orientation of the most stable adsorption complexes. The highest adsorption energy on bare ACNRs occurs when DBT is adsorbed through the hydrogen atoms ($E_A \sim -0.40$ eV) in contrast to the case when it interacts via the sulfur atom ($E_A \sim -0.23$ eV).

The relatively short bond distance (d ∼ 2.76 Å) in the H⊥ACNR configuration versus the S⊥ACNR (d ∼ 3.18 Å) configuration indicates that the bare ACNR surface does not interact directly with the S atom. A possible explanation of this behavior relies in the C atoms near charge neutrality on the ribbon surface that reduces the possibility of long-range dipole interactions and the large S–C distance prevents the formation of a covalent bond.

In contrast, in the complexes formed on B-ACNRs we find that the E_A magnitude of DBT on the B-doped ACNRs in the S⊥ACNR orientations is higher than complexes formed in the H⊥ACNR configurations, independently of the arrangement of dopants. The highest adsorption energies on B-doped ACNRs are found near the regions of highest values of $f^+(r)$. Moreover, those E_A always correspond to complexes formed in the S⊥ACNR orientation, this mean, involving mainly interactions with the sulfur atom.

In order to point out the preference of the S⊥ACNR over the H⊥ACNR, Table II also shows the difference of energy between configurations 1 and 2. From this row, negative values mean preference of the S⊥ACNR configuration over the H⊥ACNR configuration, as we can observe, the largest difference is up to 60 meV found in the complexes formed on the ACNR-*R*.

The charge depletion at B sites increases the surface preference to the sulfur atom by forming stable complexes, due to the increased capacity of the sulfur atom to interact electrostatically with the B atoms and to share its lone pairs of electrons via weak covalent interactions. A geometrical representation of these adsorbed configurations for the BC_3 and random conformations is shown in Figs. 3(a), 4(a), and 5(a).

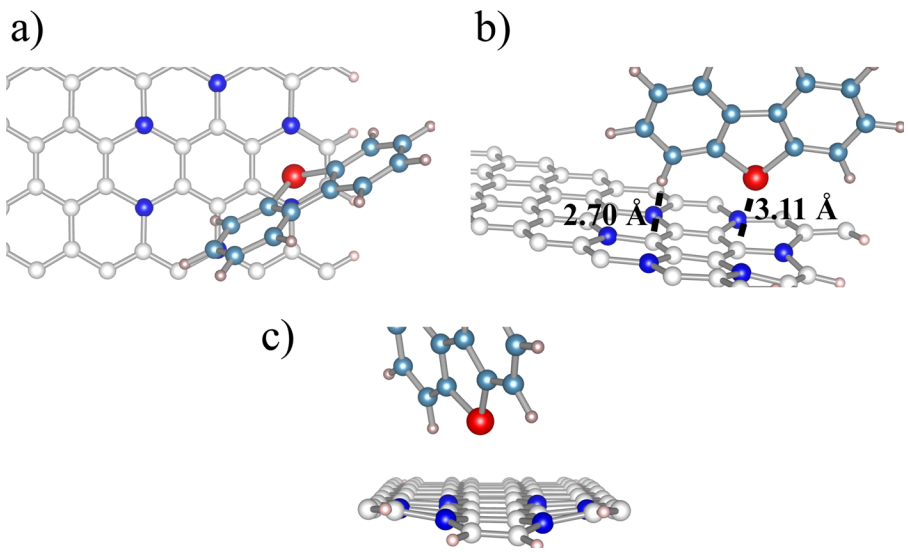

FIG. 4. Complexes formed for the DBT on the ACNR-*E* conformation. Light blue and gray balls represent carbon atoms, while boron and sulfur atoms are represented in dark blue and red colors, respectively.

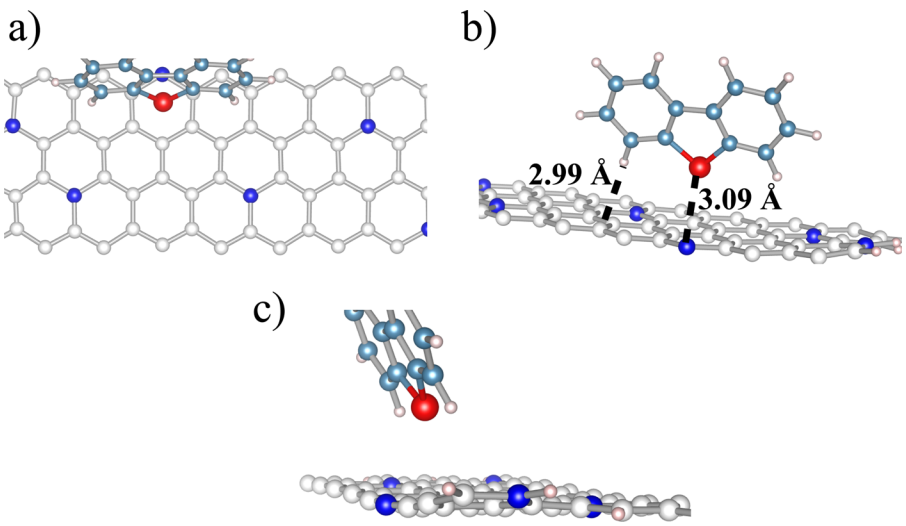

FIG. 5. Complexes formed for the DBT on the ACNR-*R* conformation. Light blue and gray balls represent carbon atoms, while boron and sulfur atoms are represented in dark blue and red colors, respectively.

The B-B interaction plays a key role in the configuration S⊥ACNR stabilization versus the H⊥ACNR ones, with the BC_3 island conformation being slightly more stable ($E_A \sim -0.42$ eV) than the random arrangement ($E_A \sim -0.40$ eV). A possible reason to explain this behavior is that in the BC_3 configuration the hydrogen atoms of carbon atoms C_4 and C_6 of the DBT molecule also interact electrostatically with C atoms nearby to the BC_3 island, increasing the adsorption energy besides the interaction of the S atom with B. This can be the reason why the DBT molecule is tilted towards B atoms in the BC_3 conformation (58.22°, see ACNR-*C* of Table II) than in the random one (67.64°, see ACNR-*R* of Table II). On the other hand, if the distance between the neighboring H atoms of the DBT molecule and the C atoms of the ribbon (with less charge depletion) is shorter, the interaction energy decreases, even if the DBT interacts directly with a complete BC_3 nanoisland (see, for instance, Fig. 4). A similar argument can explain why the H⊥ACNR configurations have less adsorption energy and are less tilted towards the B atoms than the S⊥ACNR configurations.

The E_A of the DBT on the ACNR-*C*, ACNR-*E*, and ACNR-*R* is within the conventionally accepted threshold by separating physisorption from chemisorption ($E_A \sim 0.04$–1.75 eV). Qualitatively, from an energetic point of view, the upper limit for physisorption is usually rather weak (≈0.1 eV).[55] The relatively large average strength in the S⊥ACNR configurations (d ∼ 2.95 Å) appears to be in the order of magnitude of a strong physisorption.[56]

As will be discussed in more detail in the next paragraphs, to clarify how the charge is reorganized in the complexes, the difference between the electronic charge density of the adsorbed and isolated states at position (r) is calculated as

$$\Delta\rho(\mathrm{r}) = \rho_{complex} - (\rho_{ACNR} + \rho_{DBT}), \tag{9}$$

where $\rho_{complex}$ and ρ_{ACNR} are the charge densities of the complex and isolated B-ACNRs and ρ_{DBT} is the charge density of the DBT, but with the same ionic coordinates as the total adsorbed system.

In order to analyze the nature of the DBT–ACNRs interaction, the isosurface representations as well as the $\Delta\rho$ profiles for the complexes formed by the DBT adsorbed on the ACNR-*C* and the ACNR-*R* through the S atom are shown in Fig. 6. We can observe a long range dipole interaction between the two H atoms of the C_4 and C_6 atoms of the DBT molecule with regions close to the BC_3 nanoisland of both ACNRs (see Figure 6). No net charge is observed in the $\Delta\rho$ profiles. Nevertheless, a similar charge rearrangement is observed at the DBT–ACNR interface for both cases. In addition, note from Figure 6(a) a charge accumulation in the interface of the DBT–ACNR-*C* larger than that observed in the interface of Figure 6(c) (corresponding to the ACNR-*R*). On one hand, this fact seems to indicate a slight tendency to form a covalent bonding between the S and the B atoms (see parts (a) and (b) of Figure 6), which can be related to the magnitude of the calculated E_A. However, there is charge depletion observed in both interfaces. It can help us to understand clearly the strength of the E_A, which is slightly lower in the complexes formed on the ACNR-*C* than those found in the ACNR-*R*.

Furthermore, the complexes charge transfer appears within a Bader charge distribution.[54] We find a gain of charge in the H atoms of the C_4 and C_6 of DBT, respectively, up to $0.0027\,e^-$ and $0.0098\,e^-$ during the formation of the complex on the ACNR-*C* and ACNR-*R*, respectively; while DBT sulfur atom loses charge in all the formed complexes, being up to $-0.0275\,e^-$ and $-0.0173\,e^-$ for the complexes formed on the ACNR-*C* and ACNR-*R*, respectively.

In addition, our results are in qualitative agreement with previous theoretical calculations on the adsorption of DBT and thiophene on CNTs and graphene,[55,57,58] which also found a dominating non-covalent interaction with magnitude of the adsorption energy characteristic of the physisorption process.

Taking into account the desulfurization pathways in the HDS process, organosulfur molecules are first adsorbed physically to the catalytic surface. The adsorbed states show weaker C–S bonds (characterized by longer bond distances) compared to the free molecule, which facilitates the extraction of the sulfur atom at the catalytic surface.[54,59–61] Therefore, the comparison of the C–S distances in free and adsorbed DBT states is a good indicator of the activation of the molecule upon adsorption. We found that the largest C–S

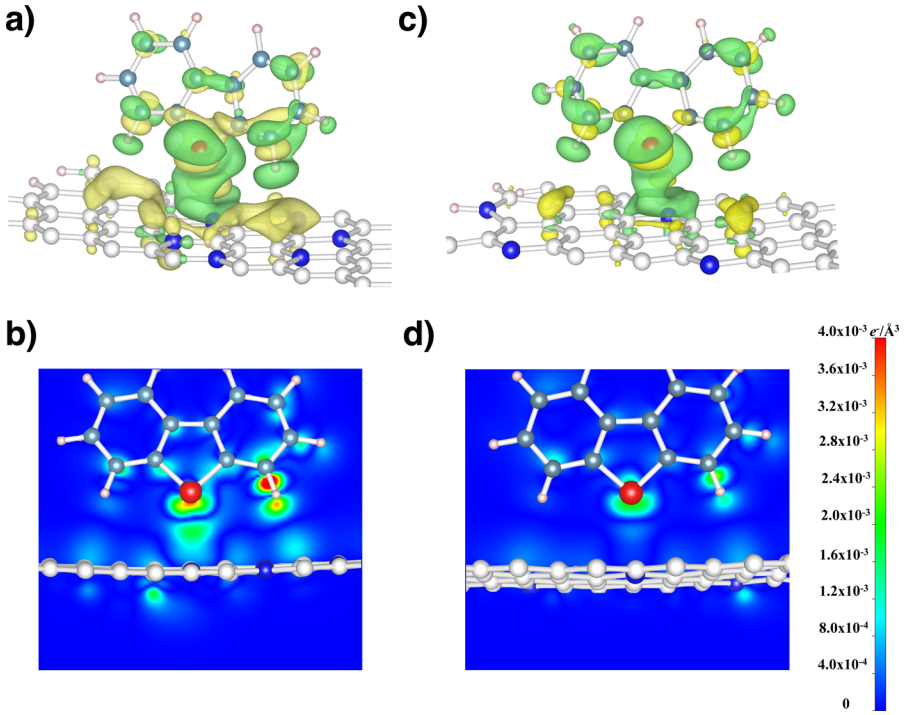

FIG. 6. Charge density difference ($\Delta\rho$) plotted of the DBT–ACNR systems. No net charge is observed in both cases but only a charge rearrangement at the DBT–ACNRs interface. Parts (a) and (c) show the $\Delta\rho$ in an isosurface representation of the complexes formed for the DBT on the ACNR-*C* and ACNR-*R*, respectively, the selected surfaces correspond to the charge isodensity of 3×10^{-4} e^-/Å and -3×10^{-4} e^-/Å, the yellow regions represent charge accumulation and the green regions indicate charge depletion. Parts (b) and (d) show a projection of the $\Delta\rho$ of the DBT on the ACNR-*C* and ACNR-*R*, respectively.

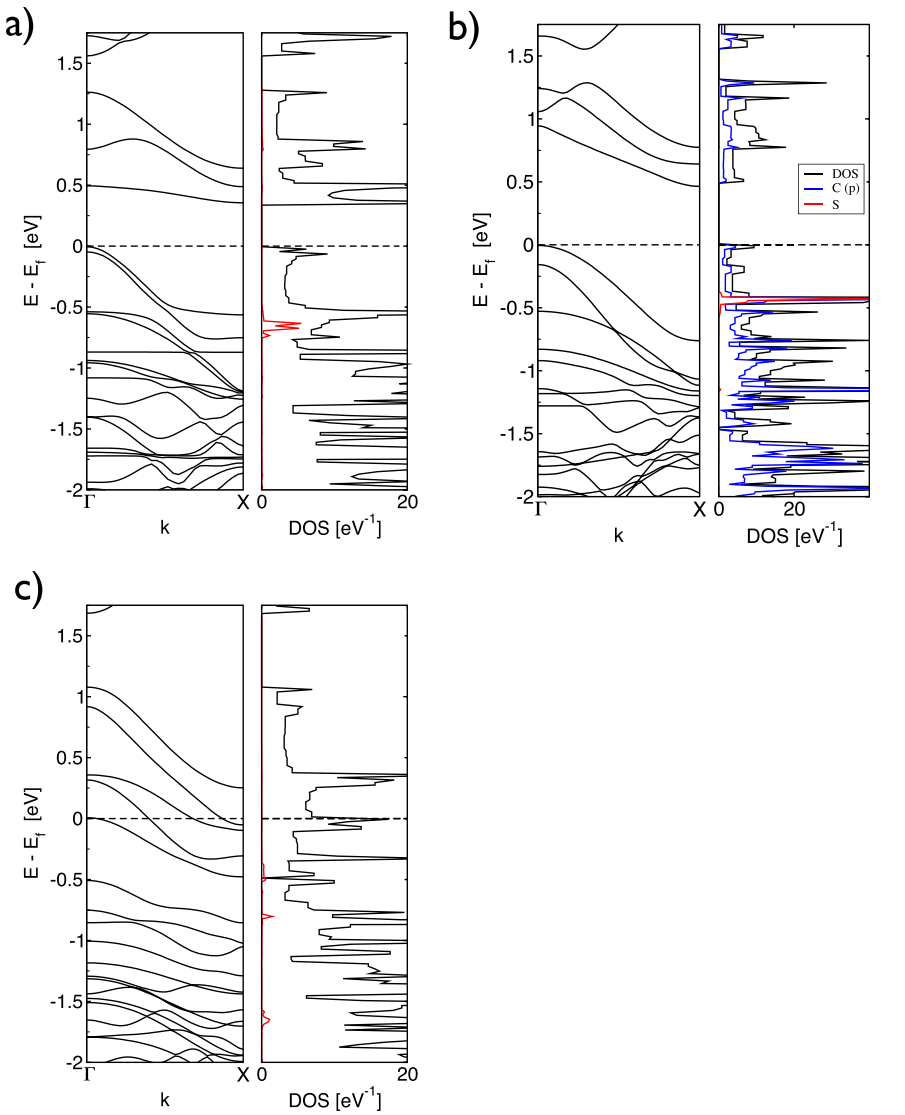

FIG. 7. Band structure, DOS, and LDOS of the nanoribbons: (a) ACNR-*C*, (b) ACNR-*E*, and (c) ACNR-*R*, respectively. Black lines: Band structure and DOS of the doped ACNR. Red lines: LDOS of the sulfur atom in the adsorbed state of the ACNR of highest adsorption energy. Blue line: LDOS of the *p* orbital of carbon atoms of the ACNR-*E*.

length corresponds to the adsorbed state on the ACNR-*C* configuration, being these separations up to 0.05 Å larger than the corresponding bond length of the free molecule. In agreement with these results, Cristol *et al.*[54] have reported that C–S length is increased up to 0.06 Å in their study for the adsorption of DBT on MoS_2 nanoclusters.

Finally, we have studied the effects of DBT on the electronic properties of the B-doped ACNRs. Figure 7 shows the band structure, total density of states (DOS), and local density of states (LDOS) of the sulfur atom in the DBT adsorption complexes of largest adsorption energy (ACNR-*C*, ACNR-*E*, and ACNR-*R*, respectively). We observe that, in general, the adsorption of DBT does not induce noticeable changes in the band structure of the ribbons near the Fermi level (E_F), i.e., it does not change in a significant way the semiconducting or metallic character of the ribbons since there is no charge transfer or covalent bonding. This behavior is in agreement with previous studies on the adsorption for thiophene on graphene.[62] However, the distribution of the S states of DBT is strongly modified by the B-B arrangement. For instance, if the DBT is adsorbed on semiconducting ACNR-*C* and ACNR-*E* conformations, its S electronic states remain strongly localized below the Fermi level [see the red curve in Figs. 7(a) and 7(b)]. Note the localized electronic states of the S atom below E_F in Figure 7(b), we suppose that those electronic states come from the charge accumulation of the surface and depletion on the either side of the hydrogen atoms of the DBT (see, for instance, the H-surface lengths in Figure 4). This fact implies a possible hybridization between the DBT and the ribbon electronic states. To understand these findings, the LDOS of the carbon atoms is included in Figure 7(b); in here, the electronic states of the S and C_4, C_6 of the DBT overlap with carbon peaks of the ACNR-*E* with some degree of hybridization.

Meanwhile, if the adsorption takes place on a metallic ACNR-*R*, there is a delocalization near E_F on the S states [see the red curve in Fig. 7(c)].

IV. CONCLUSIONS

In this work we have investigated the adsorption of DBT on bare and B-doped ACNRs in the framework of DFT by using periodic boundary conditions and including dispersion interactions. It was found that the dispersion correction is fundamental to describe the adsorption process of these systems, as the local PBE functional produces metastable complexes. Overall, our calculations suggest that the DBT interacts on the B-doped ACNRs follow a physisorption process. Although the adsorption mechanism is mainly non covalent, the introduction of charge defects by dopant atoms changes the adsorption properties by representing a convenient way to adjust the reactivity of the ribbons. The relative arrangement of the dopant atoms is another parameter that may serve to tune the electronic and chemical properties in view of potential technological applications.

ACKNOWLEDGMENTS

J. L. Ricardo-Chávez acknowledges partial support from CONACyT under Project No. CB-83642. P. Navarro-Santos thanks to CONACyT for a fellowship under the "Cátedras CONACYT" program and for GRANT No. 252239 under the Infrastructure program. Computing resources were provided by CNS-IPICyT (San Luis Potosí, Mexico) and TACC (University of Texas, USA).

[1]H. Sakurai, H. J. Tobias, K. Park, D. Zarling, K. S. Docherty, D. B. Kittelson, P. H. McMurry, and P. J. Ziemann, Atmos. Environ. **37**, 1199 (2003).
[2]Y. Wang and R. T. Yang, Langmuir **23**, 3825 (2007).
[3]V. Meille, E. Schulz, V. Meille, M. Vrinat, and M. Lemaire, Chem. Commun. **3**, 305 (1998).
[4]M. Nagai, T. Miyao, and T. Tuboi, Catal. Lett. **18**, 9 (1993).
[5]N. Nelson and R. B. Levy, J. Catal. **58**, 485 (1979).
[6]C. Song, Catal. Today **86**, 211 (2003).
[7]M. Seredych and T. J. Bandosz, Energy Fuels **24**, 3352 (2010).
[8]P. Xu, W. Xu, X. Zhang, and Y. Yan, Microchim. Acta **171**, 441 (2010).
[9]A. Srivastav and V. C. Srivastava, J. Hazard. Mater. **170**, 1133 (2009).
[10]L. Wang, Z. Sun, Y. Ding, Y. Chen, Q. Li, M. Xu, H. Li, and L. Song, Appl. Surf. Sci. **257**, 7539 (2011).
[11]M. Seredych and T. J. Bandosz, Appl. Catal., B **106**, 133 (2011).
[12]J. Xiao, G. Bian, W. Zhang, and Z. Li, J. Chem. Eng. Data **55**, 5818 (2010).
[13]C. Yu, J. Qiu, Y. Sun, X. Li, G. Chen, and Z. Zhao, J. Porous Mater. **15**, 151 (2008).
[14]S. Iijima, Nature **354**, 56 (1991).
[15]K. S. Novoselov, A. K. Geim, S. V. Morozov, D. Jiang, M. I. Katsnelson, I. V. Grigorieva, S. V. Dubonos, and A. A. Firsov, Nature **438**, 197 (2005).
[16]T. Ohta, A. Bostwick, T. Seyller, K. Horn, and E. Rotenberg, Science **313**, 951 (2006).
[17]Y. Zhang, Y.-W. Tan, H. L. Stormer, and P. Kim, Nature **438**, 201 (2005).
[18]H. S. Song, C. H. Ko, W. Ahn, B. J. Kim, E. Croiset, Z. Chen, and S. C. Nam, Ind. Eng. Chem. Res. **51**, 10259 (2012).
[19]M. Fujita, K. Wakabayashi, K. Nakada, and K. Kusakabe, J. Phys. Soc. Jpn. **65**, 1920 (1996).
[20]Y.-L. Lee and Y.-W. Lee, Phys. Rev. B **66**, 245402 (2002).
[21]Y. Miyamoto, K. Nakada, and M. Fujita, Phys. Rev. B **60**, 16211 (1999).
[22]K. Nakada, M. Fujita, G. Dresselhaus, and M. S. Dresselhaus, Phys. Rev. B **54**, 17954 (1996).
[23]Y.-W. Son, M. L. Cohen, and S. G. Louie, Phys. Rev. Lett. **97**, 216803 (2006).
[24]F. Cervantes-Sodi, G. Csányi, S. Piscanec, and A. C. Ferrari, Phys. Rev. B **77**, 165427 (2008).
[25]M. Ezawa, Phys. Rev. B **73**, 045432 (2006).
[26]P. Navarro-Santos, J. L. Ricardo-Chávez, M. Reyes-Reyes, J. L. Rivera, and R. López-Sandoval, J. Phys.: Condens. Matter **22**, 505302 (2010).
[27]See http://cms.mpi.univie.ac.at/vasp/vasp/vasp.html for relevant information of the VASP program.
[28]G. Kresse and J. Furthmüller, Phys. Rev. B **54**, 11169 (1996).
[29]G. Kresse and J. Hafner, Phys. Rev. B **47**, 558 (1993).
[30]P. E. Blöchl, Phys. Rev. B **50**, 17953 (1994).
[31]G. Kresse and D. Joubert, Phys. Rev. B **59**, 1758 (1999).
[32]S. Grimme, J. Comput. Chem. **27**, 1787 (2006).
[33]J. P. Perdew, K. Burke, and M. Ernzerhof, Phys. Rev. Lett. **77**, 3865 (1996).
[34]P. W. Ayers, F. De Proft, A. Borgoo, and P. Geerlings, J. Chem. Phys. **126**, 224107 (2007).
[35]H. Chermette, P. Boulet, and P. Stefan, *Reviews of Modern Quantum Chemistry: A Celebration of the Contributions of Robert G. Parr* (World Scientific, Singapore, 2002), Vol. II.
[36]W. Yang and W. J. Mortier, J. Am. Chem. Soc. **108**, 5708 (1986).
[37]J. L. Gazquez, *Structure and Bonding* (Springer-Verlag, Berlin, 1993).
[38]P. W. Ayers and R. G. Parr, J. Am. Chem. Soc. **122**, 2010 (2000).
[39]W. Yang and R. G. Parr, Proc. Natl. Acad. Sci. U.S.A. **82**, 6723 (1985).
[40]P. W. Ayers, W. Yang, and L. J. Bartolotti, *Chemical Reactivity Theory: A Density Functional View* (CRC Press, 2009).
[41]P. Politzer, J. S. Murray, and Z. Peralta-Inga, Int. J. Quantum Chem. **85**, 676 (2001).
[42]R. G. Pearson, J. Am. Chem. Soc. **85**, 3533 (1963).
[43]M. E. Beck, J. Chem. Inf. Model. **45**, 273 (2005).
[44]P. López and F. Méndez, Org. Lett. **6**, 1781 (2004).
[45]J. L. Rivera, J. L. Rico, and F. W. Starr, J. Phys. Chem. C **111**, 18899 (2007).
[46]K. Momma and F. Izumi, J. Appl. Crystallogr. **44**, 1272 (2011).
[47]D. L. Carroll, P. Redlich, X. Blase, J. C. Charlier, S. Curran, P. M. Ajayan, S. Roth, and M. Rühle, Phys. Rev. Lett. **81**, 2332 (1998).

[48]T. B. Martins, R. H. Miwa, A. J. R. da Silva, and A. Fazzio, Phys. Rev. Lett. **98**, 196803 (2007).
[49]S. S. Yu, W. T. Zheng, Q. B. Wen, and Q. Jiang, Carbon **46**, 537 (2008).
[50]J. L. Rivera, P. Navarro-Santos, R. Guerra-Gonzalez, and E. Lima, Int. J. Polym. Sci. **2014**, 11.
[51]J. L. Rivera, P. Navarro-Santos, L. Hernandez-Gonzalez, and R. Guerra-Gonzalez, J. Chem. **2014**, 8.
[52]R. Prins, M. Egorova, A. Röthlisberger, Y. Zhao, N. Sivasankar, and P. Kukula, Catal. Today **111**, 84 (2006).
[53]H. Yang, J. Chen, Y. Briker, R. Szynkarczuk, and Z. Ring, Catal. Today **109**, 16 (2005).
[54]S. Cristol, J.-F. Paul, E. Payen, D. Bougeard, F. Hutschka, and S. Clémendot, J. Catal. **224**, 138 (2004).
[55]B. Gómez and J. M. Martínez-Magadán, J. Phys. Chem. B **109**, 14868 (2005).
[56]C. Vasile, A. Nicolae, C. Martin, L. Predrag, and B. Stefan, J. Phys.: Condens. Matter **24**, 424214 (2012).
[57]A. Galano and M. Francisco-Márquez, Chem. Phys. **345**, 87 (2008).
[58]J. Goering and U. Burghaus, Chem. Phys. Lett. **447**, 121 (2007).
[59]K. Ahmed, S. Ali, S. Ahmed, and M. Al-Saleh, React. Kinet., Mech. Catal. **103**, 113 (2011).
[60]A. Gross, *Theoretical Surface Science: A Microscopic Perspective* (Springer, Berlin, 2009).
[61]H. Yang, J. Chen, C. Fairbridge, Y. Briker, Y. J. Zhu, and Z. Ring, Fuel Process. Technol. **85**, 1415 (2004).
[62]P. A. Denis and F. Iribarne, J. Mol. Struct.: THEOCHEM **957**, 114 (2010).